ARTICLE OPEN

Check for updates

Moldable and transferrable conductive nanocomposites for epidermal electronics

Myeong Namkoong[1], Heng Guo[1], Md Saifur Rahman[1], Daniel Wang[1], Cassandra Jane Pfeil[1], Sophia Hager[1] and Limei Tian[1]✉

Skin-inspired soft and stretchable electronic devices based on functional nanomaterials have broad applications such as health monitoring, human–machine interface, and the Internet of things. Solution-processed conductive nanocomposites have shown great promise as a building block of soft and stretchable electronic devices. However, realizing conductive nanocomposites with high conductivity, electromechanical stability, and low modulus over a large area at sub-100 µm resolution remains challenging. Here, we report a moldable, transferrable, high-performance conductive nanocomposite comprised of an interpenetrating network of silver nanowires and poly(3,4-ethylenedioxythiophene): poly(styrenesulfonate). The stacked structure of the nanocomposite synergistically integrates the complementary electrical and mechanical properties of the individual components. We patterned the nanocomposite via a simple, low-cost micromolding process and then transferred the patterned large-area electrodes onto various substrates to realize soft, skin-interfaced electrophysiological sensors. Electrophysiological signals measured using the nanocomposite electrodes exhibit a higher signal-to-noise ratio than standard gel electrodes. The nanocomposite design and fabrication approach presented here can be broadly employed for soft and stretchable electronic devices.

npj Flexible Electronics (2022)6:41 ; https://doi.org/10.1038/s41528-022-00170-y

INTRODUCTION

Recent advances in bioelectronics have led to a broad class of soft, ultrathin, stretchable wearables to measure various biophysical and biochemical signals associated with health and disease[1–7]. Soft, high-performance wearable electronic devices require materials with high conductivity, electromechanical stability, and low modulus comparable to the human skin. Conductive and stretchable composites based on inorganic/organic nanomaterials, such as metal nanoparticles, nanowires, nanoribbons, nanofibrils, and nanomeshes, have been developed to overcome the limitation of conventional conductive materials and interfaces for high-quality physiological measurements and user comfort[8–11]. Among many engineered materials, solution-processed conductive nanocomposites have shown great promise for realizing soft, ultrathin, and stretchable electronic devices owing to their tunable electrical and mechanical properties[5]. However, conductive nanocomposites with homogeneously dispersed nanofillers in a non-conductive elastomeric matrix invariably exhibit a trade-off between high conductivity (requiring high volume fraction of the nanofiller) and high stretchability (requiring low volume fraction of the nanofiller). Overcoming this fundamental trade-off through material design and processing methods is critical to advance the solution-processable, high-performance wearable devices.

In addition, simple, scalable, and efficient processing methods to pattern functional materials are important for realizing high-performance, high-density wearable electronics[4,5,12–15]. For example, large-area, epidermal electronic devices fabricated in cleanroom facilities can measure multichannel, high-resolution, electrophysiological signals over the whole scalp, chest, and forearm[13]. Various fabrication strategies have been developed to achieve skin-like wearables, including vacuum deposition, lithography, etching, and transfer printing, 'cut-and-paste' method, laser patterning, screen printing, inject printing, and direct drawing on skin[12,15–22]. However, a simple, low-cost, scalable fabrication approach for solution-processed nanomaterials over a large area at sub-100 µm resolution remains challenging.

In this work, we introduce a moldable and transferrable conductive nanocomposite thin-film comprised of an interpenetrating network of silver nanowires (AgNWs) and poly(3,4-ethylenedioxythiophene):poly(styrenesulfonate) (PEDOT:PSS). The stacked structure of the nanocomposites synergistically integrates the properties of highly conductive metal nanowires and intrinsically soft conductive polymers. We utilize a simple micromolding method to pattern the nanocomposite thin films with a feature dimension <25 µm. The patterned nanocomposite can be easily transferred onto various flexible and stretchable substrates to achieve wearable electronics with high breathability. These nanocomposites exhibit negligible change in electromechanical stability under bending and stretching, providing a robust performance of wearable sensors. The electrophysiological recordings, including electrocardiogram (ECG), electromyogram (EMG), and electrical bioimpedance (EBI), show a higher signal-to-noise ratio compared to those collected with standard Ag/AgCl gel electrodes.

RESULTS AND DISCUSSION

Design and patterning of conductive nanocomposites

In the nanocomposite design, we employed two additives, Triton X-100 and D-sorbitol, to enhance the properties of the PEDOT:PSS films (Fig. 1a). Previously, these two additives were used separately to facilitate the formation of PEDOT:PSS nanofibrils, thereby enhancing the conductivity of the PEDOT:PSS films[23,24]. Here, Triton X improves the wetting properties of the PEDOT:PSS solution and enables the uniform coating of PEDOT:PSS on hydrophobic surfaces while D-sorbitol enhances the electrical conductivity, mechanical flexibility and stretchability of the

[1]Department of Biomedical Engineering, and Center for Remote Health Technologies and Systems, Texas A&M University, College Station, TX 77843, USA.
✉email: ltian@tamu.edu

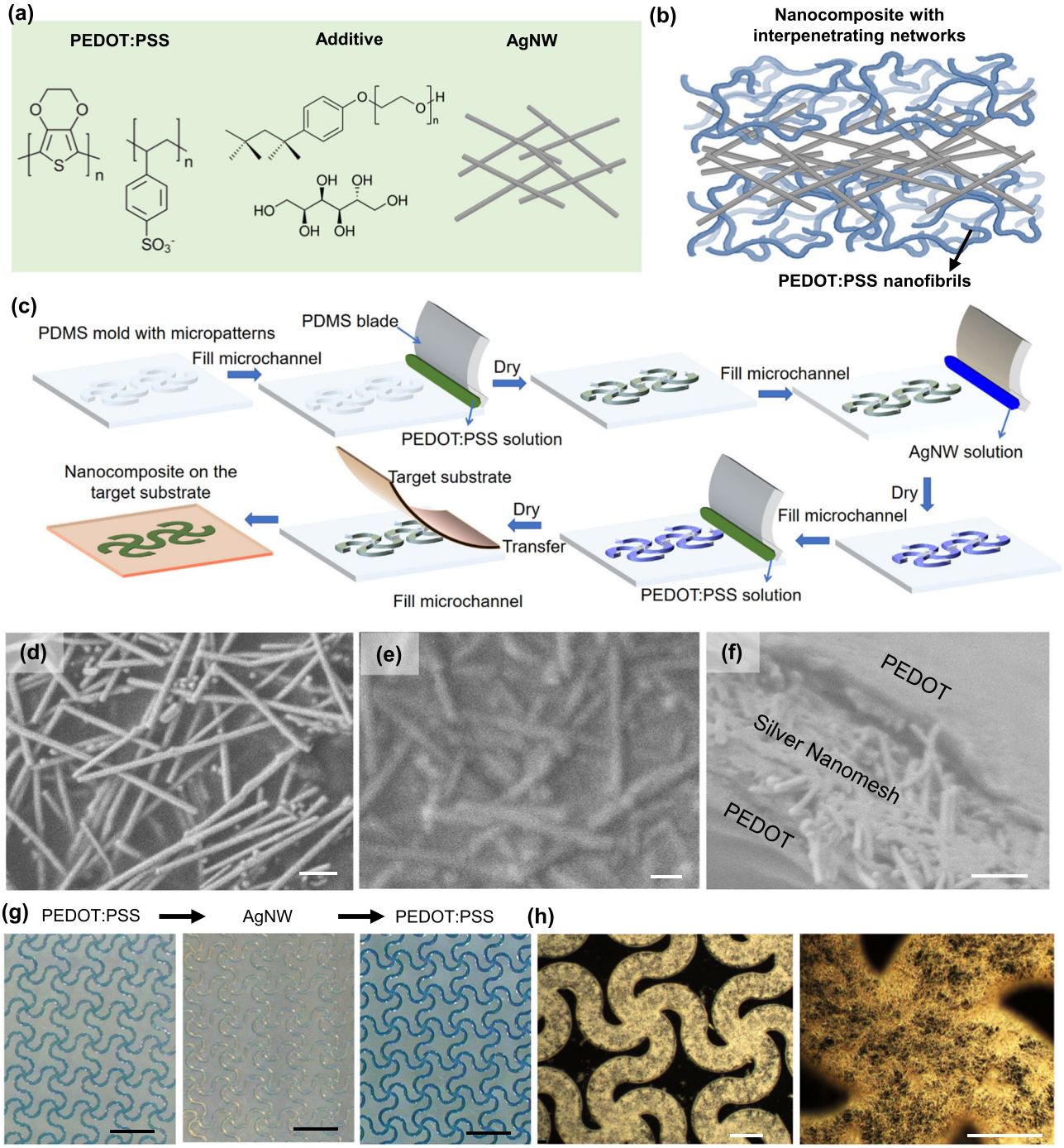

Fig. 1 Design of conductive nanocomposites. Illustrations of **a** conductive nanocomposite components, **b** cross-section structure of the nanocomposite, and **c** fabrication process. SEM images of **d** AgNWs coated on PEDOT:PSS (scale bar: 1 μm), **e** one layer of PEDOT:PSS coated on AgNWs (scale bar: 1 μm), and **f** fractured nanocomposite thin film at a tilted view (scale bar: 1 μm). **g** Bright-field optical microscope images of a PDMS mold filled with PEDOT:PSS, PEDOT:PSS/AgNW, and PEDOT:PSS/AgNW/PEDOT:PSS (scale bar: 2 mm). **h** Dark-field optical microscope images of the nanocomposite (scale bar in left: 200 μm; right: 100 μm).

PEDOT:PSS films. AgNWs are interconnected, yielding a nanomesh structure. The nanomesh design improves gas permeability and stretchability of the nanocomposite. Silver nanomesh (AgNM) and PEDOT:PSS nanofibrils form interpenetrating networks, offering high electrical conductivity and electromechanical stability of the nanocomposites (Fig. 1b). The stacked structure of the nanocomposite provides a soft and smooth PEDOT:PSS surface to contact the skin and yields a low electrical interface impedance due to the combined high ionic and electronic conductivity.

We patterned solution-processed nanomaterials via a simple, low-cost micromolding process and then transferred print the patterned nanocomposites on various substrates to achieve nanocomposite electrophysiological sensors (Fig. 1c). Compared to previously reported micromolding in capillaries, this approach does not require the mold placed on a support to form microchannels, thereby allowing for the fabrication of nanocomposites with any desired micropatterns, including the non-interconnected patterns[25,26]. The fabrication steps include (i)

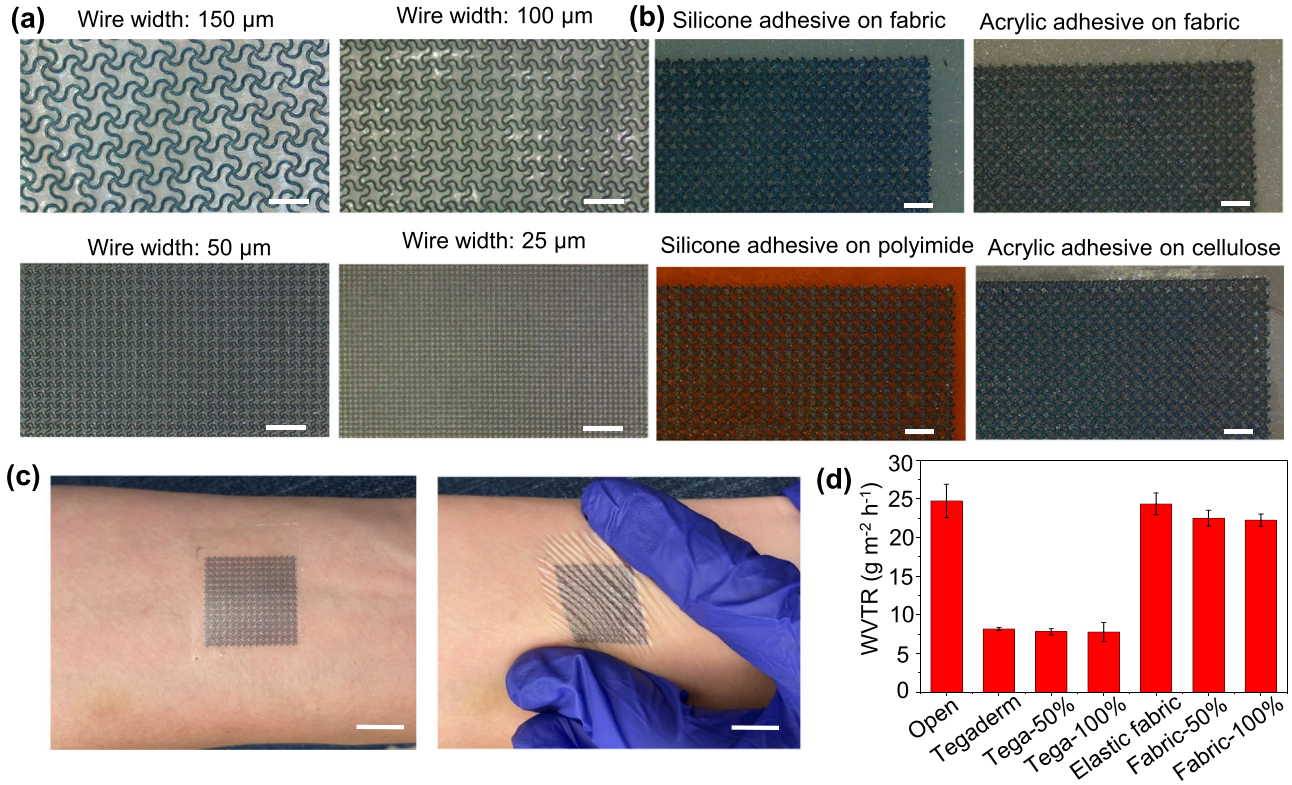

Fig. 2 Transfer printing of nanocomposite thin films. a Optical microscope images of nanocomposite patterns with different wire widths from 25 to 150 μm, transferred onto a 3M Tegaderm adhesive (scale bar: 2 mm). **b** Optical microscope images of nanocomposite electrodes of 50% fill factor transferred onto silicone and acrylic adhesives on different types of substrates (scale bar: 2 mm). **c** Photographs of a nanocomposite electrode laminated on the human skin under rest and compression (scale bar: 1 cm). **d** Water vapor transmission rate (WVTR) comparison of nanocomposite thin films on medical adhesives with different breathability and open bottle control. The error bar represents the standard deviation from three samples.

preparation of a polydimethylsiloxane (PDMS) mold with desired micropatterns, (ii) filling the microchannel with PEDOT:PSS solution with a PDMS blade, (iii) film drying at 60 °C for 5 min, (iv) repeating the steps (ii) and (iii) with AgNW solution and PEDOT:PSS solution, followed by annealing at 130 °C for 30 min, and (v) transferring the composite to a target substrate. The width of the microchannel in the PDMS mold ranges from 25 to 250 μm, and the depth is ~50 μm (Supplementary Fig. 1). The PDMS mold can be reused. The pristine PEDOT:PSS aqueous solution does not uniformly fill the PDMS microchannels after blading due to the poor wetting of the PEDOT:PSS solution on the hydrophobic surface (Supplementary Fig. 2a). A small amount of a nonionic surfactant (Triton X, 3 wt%) was added to achieve uniform filling (Supplementary Fig. 2b). The addition of Triton-X reduces the contact angle of the PEDOT:PSS solution on the PDMS surface from 122° to 77°, confirming the improved wetting (Supplementary Fig. 3). It is important to note that Triton X also reduces the interfacial adhesion between the PEDOT film and the PDMS, enabling the easy transfer of the film onto various target substrates. In this fabrication approach, once the PDMS mold is prepared, the following nanocomposite patterning does not rely on standard microfabrication procedures, including vacuum deposition, spin coating, photolithography, wet and dry etching. In addition, compared to the subtractive manufacturing process, it minimizes materials waste.

The nanocomposite thickness can be tuned by the concentration of the precursor solutions and the number of blading depositions. Twice depositions of each layer yield ~1.2 μm-thick nanocomposite (Supplementary Fig. 4b). The dimension and density of AgNWs can tune the conductivity of the nanocomposite according to percolation studies[27,28]. After coating AgNWs on the PEDOT:PSS, a scanning electron microscope (SEM) image reveals the uniform distribution of AgNWs with a diameter of ~250 nm and a length of 10–20 μm and the interpenetrating interface between AgNWs and PEDOT:PSS layer (Fig. 1d)[29,30]. SEM image of the nanocomposite after one-time deposition of the PEDOT:PSS on AgNWs shows a rough surface topography following the AgNM underneath. A tilted SEM image shows the nanocomposite surface becomes smooth after the second deposition of the PEDOT:PSS (Fig. 1e). The image also confirms the stacked structure of the nanocomposite with an AgNM sandwiched between PEDOT:PSS layers (Fig. 1e). The cross-section SEM image of the nanocomposite further confirms that the PEDOT:PSS and AgNM form an interpenetrating network to yield a mechanically stable nanocomposite (Supplementary Fig. 4b). Figure 1g shows optical microscope images of a PDMS mold filled with PEDOT:PSS, AgNW, and PEDOT:PSS subsequently after drying. The color changes from uniform light blue to light yellow to deep blue following each deposition. Dark-field optical microscope images further confirm the uniform distribution and interconnected structure of AgNWs (Fig. 1h).

Transfer printing of nanocomposite thin films

Current low-cost methods to pattern AgNWs include screen printing and stencil printing, which yield the feature dimension mostly larger than 100 μm[31,32]. The micropatterning strategy described above can produce ultrathin nanocomposites of arbitrary and complex geometries with a feature dimension <25 μm. The optical microscope images show nanocomposite serpentine patterns with a 30% fill factor (effective conductive area/electrode area) transferred on 3M Tegaderm adhesives (Fig. 2a and Supplementary Fig. 5). The wire width of the nanocomposite

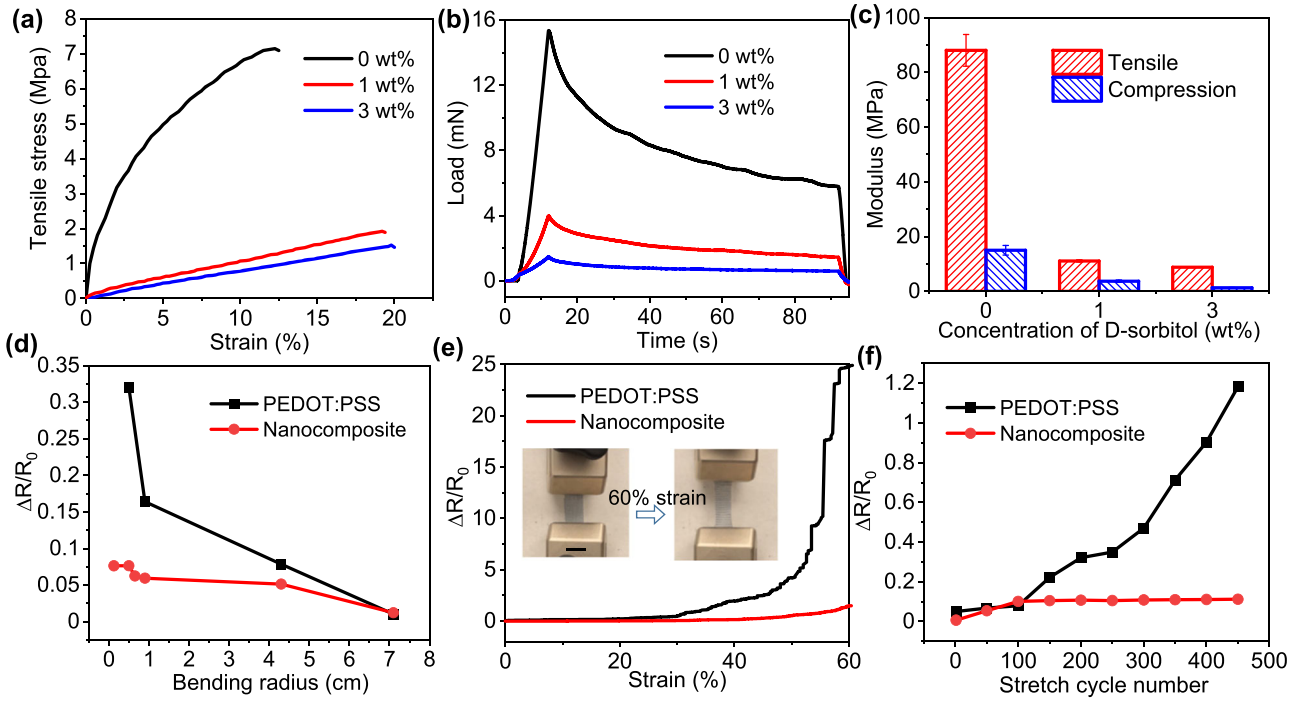

Fig. 3 Electromechanical characterization of nanocomposite thin films. a Tensile stress–strain curves and **b** stress relaxation curves of PEDOT:PSS films prepared with 3 wt% Triton X and varying concentrations of D-sorbitol from 0 to 3 wt%. **c** Elastic moduli comparison of the PEDOT:PSS films calculated from (**a**) and (**b**). Resistance changes in the serpentine nanocomposite and PEDOT:PSS thin films **d** under bending, **e** under stretching (scale bar: 1 cm), and **f** after numerous stretch and release cycles. The error bar represents the standard deviation from three samples.

filaments ranges from 150 to 25 µm. With this facile fabrication approach, the patterned nanocomposite can easily integrate with common adhesive substrates to yield electronic devices with different adhesion and breathability based on the user preference and applications. Figure 2b and Supplementary Fig. 6 show the nanocomposite patterns with a wire width of 150 µm over a centimeter-scale area transferred onto various substrates, including silicone adhesives on polyimide and fabric substrates and acrylic adhesives on fabric and water-soluble cellulose paper. Silicone adhesives provide mild adhesion to the skin, ideal for people with sensitive skin or scarred skin[33]. In contrast, acrylic adhesives provide strong adhesion to the skin, thereby more traumatic to the skin during removal.

Figure 2c shows photographs of a representative nanocomposite electrode with a serpentine pattern laminated on the forearm at rest and compressed state. The electrode follows the natural deformation of the skin without constraint or delamination, confirming its good conformability to the skin. Previously reported gas-permeable electrodes and substrates have significantly improved perspiration transport and evaporation, thereby minimizing skin irritation and inflammation risks after long-term wear[6,13,17,34,35]. To evaluate the breathability of the nanocomposite, we measured water vapor transmission rate (WVTR) through the nanocomposite laminated on the medical-grade adhesive substrates with different breathability (Fig. 2d). With different substrates, properties that range from full breathability to constrained transdermal loss can be achieved. The 3M Tegaderm shows three times lower WVTR than the value determined without any cover layer, shown as the open case in the results. The elastic nonwoven fabric medical tape (3M 9907W) is highly breathable with a similar WVTR as the open case. The nanocomposite with a serpentine pattern of 50% fill factor (conductive area/electrode area) and with 100% fill factor (a fully covered film) on both substrates show <10% decrease in WVTR than that measured from the substrates only. These results suggest that the nanocomposite has a negligible effect on the WVTR of the devices.

Electromechanical characterization of nanocomposite thin films

To validate the electromechanical stability of nanocomposite thin films, we first investigated the effect of dual additives, i.e., Triton X and D-sorbitol, on the mechanical and electrical properties of PEDOT:PSS films. Figure 3a shows the stress–strain curves of PEDOT:PSS films with 3 wt% Triton X and varying concentrations of D-sorbitol from 0 to 3 wt%, obtained by uniaxial tensile testing. With the increase of D-sorbitol, the elongation of the PEDOT:PSS films at break increases while Young's modulus decreases. The PEDOT:PSS film without D-sorbitol exhibit an elongation of ~12% at the break, Young's modulus of ~88 MPa, and tensile strength of ~7 MPa. The addition of D-sorbitol significantly decreases Young's modulus of the PEDOT:PSS films. The tensile strength decreases from 1.9 to 1.5 MPa, and Young's modulus decreases from 11.1 to 8.8 MPa, with the concentration of D-sorbitol increasing from 1 to 3 wt%. The elastic modulus of the PEDOT films was also measured by microindentation tests. The stress relaxation curves characterize the viscoelastic behavior of the PEDOT:PSS films (Fig. 3b). The hold segments were fitted using a two-exponent exponential decay equation to determine the load at equilibrium (Supplementary Fig. 7)[36]. The calculated elastic modulus of the PEDOT:PSS films decreases from 15.0 to 1.7 Mpa with increasing the concentration of D-sorbitol from 0 to 3 wt%. The elastic modulus determined by indentation tests is 3–6 times lower than the tensile modulus, which likely results from the preferential alignment of PEDOT:PSS nanofibrils parallel to the film plane. The elastic moduli of the skin at different body locations and orientations range from 0.54 to 1.95 MPa[37]. These results show that the modulus of the PEDOT:PSS film with D-sorbitol is comparable with that of the skin, which can facilitate its conformal contact with the skin.

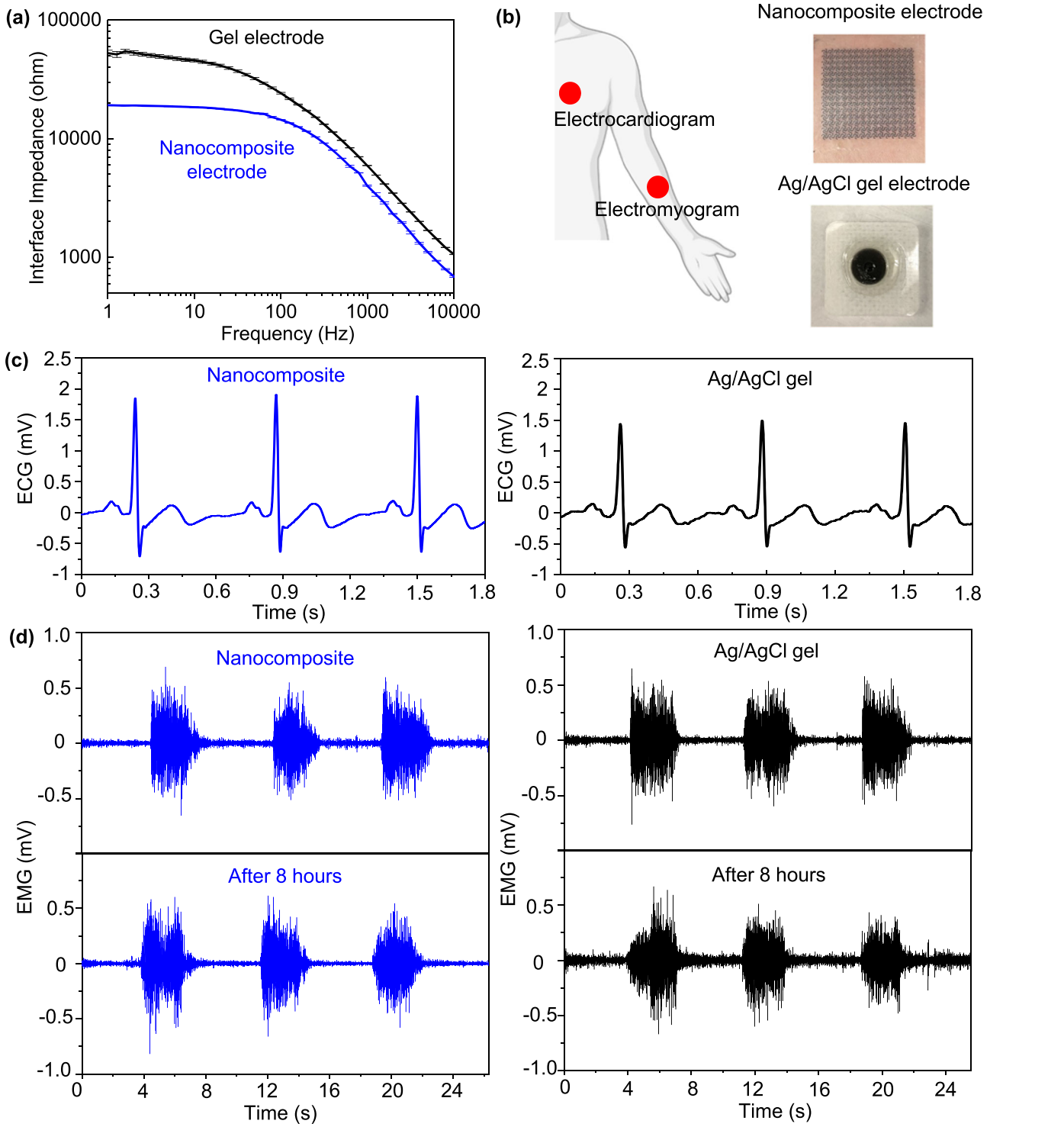

Fig. 4 ECG and EMG recordings. a Comparison of the skin–electrode interface electrical impedance measured with conventional Ag/AgCl gel electrodes and nanocomposite electrodes. **b** Schematic illustration of sensor locations for ECG and EMG recordings and photographs of nanocomposite and gel electrodes. **c** ECG signals measured with nanocomposite and gel electrodes. **d** EMG signals measured with nanocomposite mesh and gel electrodes before and after wearing for 8 h.

The conductivity of the PEDOT:PSS films with 3 wt% Triton X was measured to be ~93 S/cm. It increased to ~167 S/cm with the addition of 3 wt% D-sorbitol. We prepared conductive nanocomposite films with a serpentine pattern of 50% fill factor, 150 μm wire width, and ~1.2 μm thickness using the PEDOT:PSS solution with 3 wt% Triton X and 3 wt% D-sorbitol for the following measurements. The sheet resistance of ~1.2 μm thick nanocomposite serpentine film is ~70 Ω/sq, much lower than that of the PEDOT:PSS film without AgNWs (~120 Ω/sq). We evaluated the electromechanical stability of the nanocomposite films by measuring the resistance changes under bending and stretching and compared them with those of the films without AgNWs. The bending tests were performed by wrapping thin films on the cylinders with varying radii from 0.125 to 7 mm. The resistance of

the thin films increases under bending with decreasing the bending radius (Fig. 3d). The nanocomposite films exhibit less than an 8% increase in the resistance under bending, much smaller than that of the PEDOT:PSS films. Under uniaxial stretch, the resistance of the nanocomposite films increases by 5% under 30% strain and 1.5 times under 60% strain (Fig. 3e). In contrast, the resistance of PEDOT:PSS films increases by 50% under 30% strain and 24.8 times under 60% strain, much higher than the resistance change of the nanocomposite. Cyclic stretch and release tests at 30% strain were performed to evaluate the electromechanical stability and durability of the nanocomposite film. The resistance increase of the nanocomposite is ~11% after 450 stretch and release cycles, much lower than the resistance increase ~118% of the PEDOT:PSS film (Fig. 3f).

Electrophysiological monitoring with nanocomposite sensors

Previously developed epidermal electrophysiological sensors with optimal mechanics design provide comparable signal quality to standard Ag/AgCl gel electrodes[6,9,13,19,38]. In contrast, our nanocomposite sensors provide a lower skin–electrode interface impedance and a higher signal-to-noise ratio than the standards. We used electrochemical impedance spectroscopy to measure the skin–electrode interface impedance as a function of frequency. We compared the interface impedance measured with nanocomposite electrodes and standard Ag/AgCl gel electrodes (Fig. 4a). The effective conductive area of nanocomposite electrodes is around 0.9 cm^2, approximately half of the conductive gel area of Ag/AgCl electrodes. The interface impedance decreases with increasing the frequency from 1 Hz to 10 kHz, relevant to the frequency of electrophysiological signals. The impedance with Ag/AgCl gel electrodes is 2.8 times higher at 1 Hz and 1.7 times higher at 100 Hz than those measured with nanocomposite electrodes. The lower interface impedance of the nanocomposite electrodes mainly results from the combined high ionic and electronic conductivity of the PEDOT:PSS and AgNM.

We demonstrate that nanocomposite electrodes can provide robust electrocardiogram (ECG), electromyogram (EMG), and bioimpedance recordings. ECG records the electrical activity of the heart. It is a standard test for detecting numerous cardiac abnormalities, such as atrial fibrillation and myocardial infarction[39]. EMG measures the electrical activity of skeletal muscles, which can evaluate the function of muscles and the nerve cells

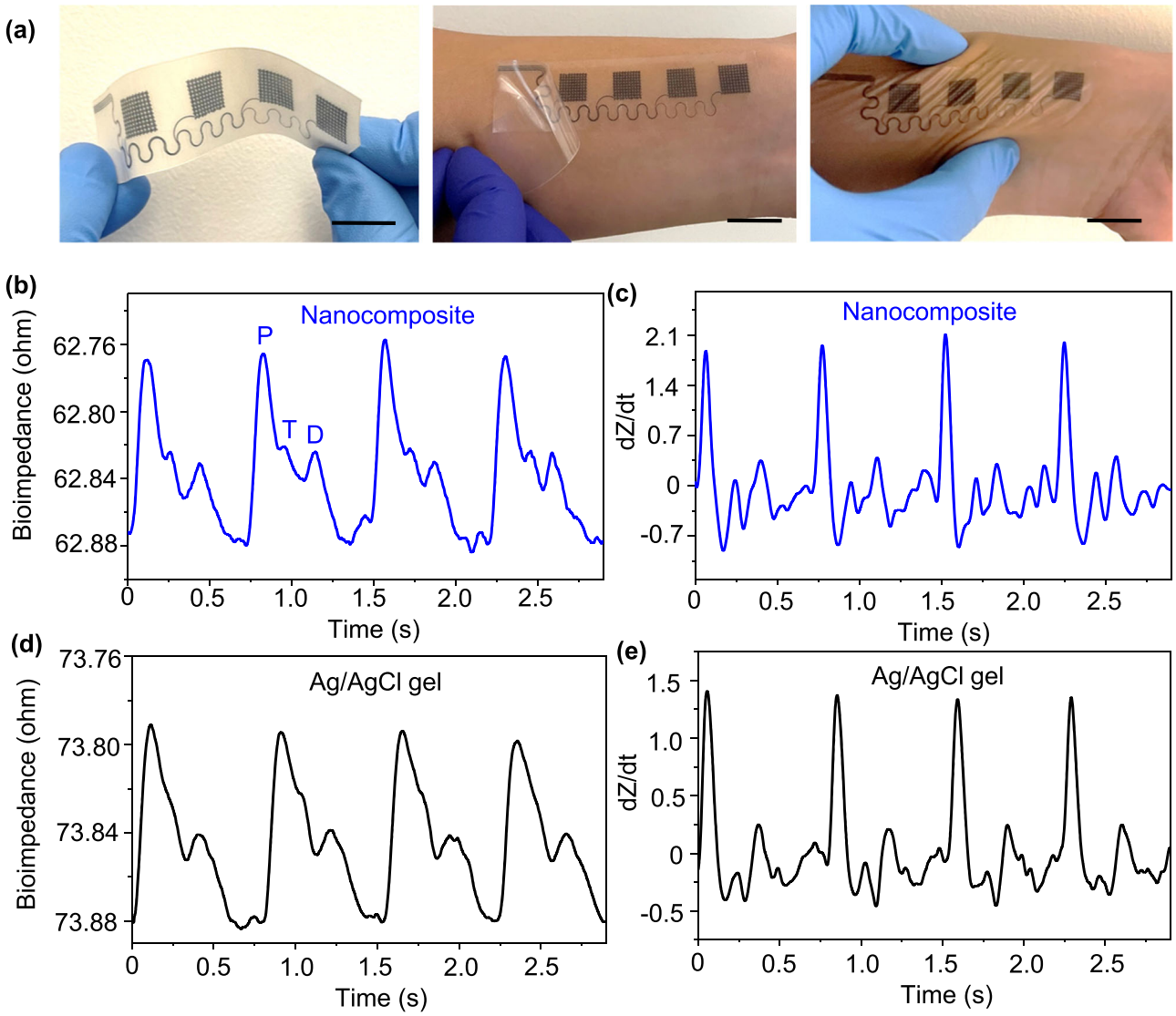

Fig. 5 Bioimpedance measurements. a Photograph of a nanocomposite electrode array transferred on a medical adhesive and laminated on the forearm before and after removing the temporary support (scale bar: 2 cm). **b** Bioimpedance signals and **c** the first derivative with respect to time measured with nanocomposite electrodes. **d** Bioimpedance signals and **e** the first derivative measured with gel electrodes.

that control them and serve as an input signal for human–machine interaction[40]. To compare the performance of nanocomposite and standard Ag/AgCl gel electrodes for these recordings, we mounted the electrodes onto a human subject's chest for ECG and forearm for EMG (Fig. 4b). Figure 4c shows the ECG signals collected with nanocomposite and gel electrodes. Both waveforms reveal important features of ECG, including P wave, QRS complex, and T-wave. The nanocomposite electrodes provide ECG signals with a peak-to-peak voltage of 2.56 mV, higher than that collected with gel electrodes (2 mV). To measure EMG, we placed a pair of electrodes on the flexor muscles of the forearm to measure the muscle contract intensity induced by a fixed gripping force. Figure 4d shows the EMG signals measured with nanocomposite electrodes and gel electrodes following three cycles of muscle contractions for 3 s and rest for 5 s. The signal and noise of EMG recordings are calculated from the rectified voltages induced by muscle contractions and at rest state, using the root-mean-squared (RMS) analysis. The RMS noise with the nanocomposite electrodes is 10.3 μV, close to that of gel electrodes (10.6 μV). The signal-to-noise ratio of EMG signals with nanocomposite electrodes is 10.9 dB, also comparable with gel electrodes (10.6 dB). However, after the human subject wore the electrodes for 8 h, the noise with the gel electrodes increased to 18.6 μV, and the signal-to-noise ratio decreased to 7.5 dB. In contrast, the signal quality of EMG measured with the nanocomposite electrodes improved over time, with the noise decreased to 7.3 μV, and the signal-to-noise ratio increased to 12.3 dB. The improved signal quality likely resulted from the increased ionic conductivity of the nanocomposites after 8 h of wearing.

To demonstrate large-area electrophysiological sensing, we fabricated an array of nanocomposite electrodes with an overall dimension of 2 cm × 8 cm and individual electrodes of 1 cm × 1 cm for bioimpedance recordings on the wrist. Bioimpedance measurement is a promising approach to obtain the pulse waveform that continuously reflects the blood pressure changes through the impedance change in the local artery. Previous studies rely on rigid electrodes to measure bioimpedance and show that the electrode–skin impedance with rigid electrodes is much higher than that with gel electrodes[41,42]. The nanocomposite electrodes reported in this work provide lower interface impedance and higher signal quality than gel electrodes. Figure 5a shows an electrode array laminated on the wrist along the radial artery for bioimpedance measurements with a four-probe configuration. Two outer electrodes inject a small alternating current of 400 μA at 100 kHz while two inner electrodes measure the voltage change over time. Figure 5b shows bioimpedance recording over four pulse periods measured with nanocomposite electrodes. The derivative of the impedance magnitude dZ/dt was calculated and shown with positive polarity (Fig. 5c). The derivative of the bioimpedance can be used to quantify basic hemodynamic parameters, such as stroke volume and cardiac output[43]. A characteristic bioimpedance pulse waveform exhibits three distinguishable peaks, including the Percussion wave (P wave), the Tidal wave (T wave), and the Dicrotic wave (D wave)[44]. These peaks result from the ejection of blood from the left ventricle into the aorta, reflected waves from the hand and the lower body, and the aortic valve closure. The bioimpedance waveform measured with nanocomposite sensors clearly exhibits these three peaks. The radial augmentation index AI_r (amplitude of P wave/amplitude of T wave) can diagnose arterial stiffness[44]. In our measurements, the AI_r is calculated to be ~49%, consistent with the value reported for a healthy adult male of 25 years old[44]. In contrast, gel electrodes show a higher impedance magnitude than nanocomposite electrodes (Fig. 5d). The T wave is not clearly distinguishable in the bioimpedance waveform collected with the gel electrodes. In addition, the dZ/dt derived from the nanocomposite sensors is 1.7 times larger than the gel system (Fig. 5c, e). These results collectively confirm the higher quality of electrophysiological signals measured using nanocomposite sensors, compared to standard gel electrodes.

In summary, we have introduced moldable and transferrable conductive nanocomposites that leverage synergistic properties of AgNWs and PEDOT:PSS for soft and stretchable skin–interfaced electronic devices. A simple, low-cost micromolding approach can pattern solution-processed nanocomposites with a feature dimension <25 μm. The patterned nanocomposite thin films can be transferred onto various substrates to realize electronic devices with high breathability. The electromechanical stability of the nanocomposites was validated by bending and stretching measurements. The electrophysiological signals collected with the nanocomposite sensors exhibit a higher signal-to-noise ratio than those with standard gel sensors. The nanocomposite design and fabrication strategy introduced here can be broadly employed for realizing various soft and stretchable devices, such as wearable sensors and actuators.

METHODS

Materials

Poly(3,4-ethylenedioxythiophene): poly(styrenesulfonate) was purchased from Ossila Ltd. Triton X-100, ethyl glycol, silver nitrate, polyvinylpyrrolidone (PVP, Mw = 59,000), copper chloride, D-sorbitol, and 1H,1H,2H,2H-perfluorooctyltrichlorosilane (FDTS) were purchased from Fisher Scientific. Polydimethylsiloxane (PDMS, Sylgard184) was obtained from Dow Corning. SU-8 and its developer were obtained from Kayaku Advanced Materials, Inc. All chemicals were used as purchased.

Synthesis of silver nanowire

AgNWs with a diameter of ~250 nm and a length of 10–20 μm were synthesized using a previously reported polyol method with slight modifications[29,30]. PVP (0.3 M, 10 mL), silver nitrate (0.3 M, 2 mL), and copper chloride (0.015 M, 0.02 mL) solutions were prepared using ethyl glycol (EG) as a solvent. The PVP solution was heated at 170 °C for 0.5 h. Subsequently, copper chloride and silver nitrate solutions were added under stirring and left for 50 min for silver nanowires to grow. The AgNW solution was then quenched in an ice-cold bath and centrifuged at 8000 RPM for 30 min to remove the supernatant and dispersed in ethanol for future usage.

Preparation of PDMS molds

SU-8 masters were fabricated on 4-inch silicon wafers using photolithography. First, a silicon wafer is cleaned and coated with SU-8 2050 to achieve a thickness of ~50 μm. The coated wafer was then heated at 65 °C for 3 min and 95 °C for 9 min on a hot plate. Once the wafer cooled down, it was exposed to UV energy of 200 mJ/cm^2 and heated similarly to the pre-bake protocol. The SU-8 photoresist was developed using a SU-8 developer with 4 min of agitation. The wafer was finally rinsed with IPA. Next, the SU-8 master was treated with FDTS vapor in a vacuum container for 30 min to reduce the adhesive between SU-8 and PDMS. PDMS was poured onto the wafer and placed under a vacuum for an hour to remove any air bubbles. Lastly, PDMS was cured at 60 °C for 2 h in an oven and then removed from the SU-8 master.

Fabrication of electrodes

A conductive nanocomposite electrode comprises three layers, including top and bottom PEDOT:PSS and middle AgNW layers. Following steps described in Fig. 2a, PEDOT:PSS and AgNW solutions sequentially filled the channel in a PDMS mold, followed by removing access solution with a PDMS blade and drying at 60 °C for 5 min to remove solvents. The PEDOT:PSS solution was blended with Triton X (3 wt%) and a varying amount of D-sorbitol (0–3 wt%). We systematically investigated the correlation between ink concentration and nanocomposite film thickness. The concentration of the PEDOT:PSS solution varies from 0.5 to 2.0 wt%, and the concentration of AgNW solution varies from 1.9 to 7.4 wt%. The thickness of the nanocomposite films prepared using 1.0 wt % PEDOT:PSS and 3.7 wt% AgNW solutions is around 1.2 μm. The thickness of the nanocomposite decreases to 0.49 μm with 0.5 wt% PEDOT:PSS and 1.9 wt% AgNW solutions and increases to 1.8 μm with

2.0 wt% PEDOT:PSS and 7.4 wt% AgNW solutions. These data show that the nanocomposite thickness increases with increasing ink concentration. Once the coating of all the layers was complete, the electrodes were annealed at 130 °C for 30 min. The electrodes were transferred onto adhesives after pressing the adhesive laminated on the PDMS mold with a tweezer and peeling off the adhesive from the mold. The transferred electrodes can be cut into different dimensions for further measurements. Finally, anisotropic conductive films were used to connect the electrodes to data acquisition systems.

Materials characterization

SEM images were recorded on an ultrahigh-resolution field emission scanning electron microscope (JEOL JSM-7500F). The tensile stretch and cyclic stretch and release measurements were conducted using MARK-10. The strain was applied at the rate of 5 mm/min in tensile measurements. In microindentation tests, the elastic modulus was calculated using Hertzian equation:

$$E = \frac{3}{4\sqrt{R}} \frac{1 - v^2}{h^{3/2}} \gamma_o \quad (1)$$

where γ_o represents the load at equilibrium, E is the effective elastic modulus, R is the spherical probe's radius, h is the displacement, and v is the Poisson's ratio of the sample (Supplementary Fig. 8). The thin film resistance was recorded with a digital multimeter (NI-USB4065) using a four-probe method. The skin–electrode impedance was measured with a potentiostat (Gamry).

Electrophysiological measurements

Electrocardiography (ECG) and electromyography (EMG) were measured using the BIOPAC system (MP160, ECG 100D, and EMG 100D). Three electrodes, including an anode, cathode, and ground electrodes, were attached around the heart for ECG measurements. Bipolar EMG signals were collected with two electrodes on the forearms and one ground electrode on the elbow to measure the intensity of brachioradialis muscle contraction. The electrodes were connected to the data acquisition system via anisotropic conductive films (ACF), an intermediate printed circuit board (PCB), and wires (Supplementary Fig. 9). The ACF was laminated onto the edge of the electrode pattern and applied with heat and pressure to create a robust electrical and mechanical interface between the PCB and the electrode. Bioimpedance signals were obtained using BIOPAC (MP160 and NICO100C). Four electrodes were placed along the radial artery close to the wrist on the forearm. The two outer electrodes inject a small current of 400 μA, while the two inner electrodes measure the voltage and convert it to the impedance. A 10 Hz low-pass filter and DC high-pass filter were applied in the bioimpedance measurements. All experiments involving human subjects were conducted under approval from the Institutional Review Board at Texas A&M University (project number: 118141). Briefly, healthy subjects were recruited, informed consent including publication of human subject photographs was obtained after the procedure, and the potential risks of the study were explained.

DATA AVAILABILITY

All data needed to evaluate the conclusions in the paper are present in the paper and/or the Supplementary Materials.

Received: 13 December 2021; Accepted: 10 May 2022;
Published online: 07 June 2022

REFERENCES

1. Heikenfeld, J. et al. Wearable sensors: modalities, challenges, and prospects. *Lab Chip* **18**, 217–248 (2018).
2. Ray, T. R. et al. Bio-Integrated wearable systems: a comprehensive review. *Chem. Rev.* **119**, 5461–5533 (2019).
3. Liu, Y., Pharr, M. & Salvatore, G. A. Lab-on-skin: a review of flexible and stretchable electronics for wearable health monitoring. *ACS Nano* **11**, 9614–9635 (2017).
4. Choi, S. et al. Highly conductive, stretchable and biocompatible Ag–Au core-sheath nanowire composite for wearable and implantable bioelectronics. *Nat. Nanotechnol.* **13**, 1048–1056 (2018).
5. Choi, S., Han, S. I., Kim, D., Hyeon, T. & Kim, D. H. High-performance stretchable conductive nanocomposites: materials, processes, and device applications. *Chem. Soc. Rev.* **48**, 1566–1595 (2019).
6. Miyamoto, A. et al. Inflammation-free, gas-permeable, lightweight, stretchable on-skin electronics with nanomeshes. *Nat. Nanotechnol.* **12**, 907–913 (2017).
7. Lee, S. et al. Nanomesh pressure sensor for monitoring finger manipulation without sensory interference. *Science* **370**, 966–970 (2020).
8. Rogers, J. A., Someya, T. & Huang, Y. Materials and mechanics for stretchable electronics. *Science* **327**, 1603–1607 (2010).
9. Kim, D.-H. et al. Epidermal electronics. *Science* **333**, 838–843 (2011).
10. Lipomi, D. J. et al. Skin-like pressure and strain sensors based on transparent elastic films of carbon nanotubes. *Nat. Nanotechnol.* **6**, 788–792 (2011).
11. Jang, H. et al. Graphene-based flexible and stretchable electronics. *Adv. Mater.* **28**, 4184–4202 (2016).
12. Yeo, W.-H. et al. Multifunctional epidermal electronics printed directly onto the skin. *Adv. Mater.* **25**, 2773–2778 (2013).
13. Tian, L. et al. Large-area MRI-compatible epidermal electronic interfaces for prosthetic control and cognitive monitoring. *Nat. Biotechnol.* **3**, 194–205 (2019).
14. Wang, Y. H. et al. Electrically compensated, tattoo-like electrodes for epidermal electrophysiology at scale. *Sci. Adv.* **6**, eabd0996 (2020).
15. Chandra, S. et al. Performance evaluation of a wearable tattoo electrode suitable for high-resolution surface electromyogram recording. *IEEE Trans. Biomed. Eng.* **68**, 1389–1398 (2021).
16. Yang, S. et al. "Cut-and-paste" manufacture of multiparametric epidermal sensor systems. *Adv. Mater.* **27**, 6423–6430 (2015).
17. Sun, B. et al. Gas-permeable, multifunctional on-skin electronics based on laser-induced porous graphene and sugar-templated elastomer sponges. *Adv. Mater.* **30**, 1804327 (2018).
18. Ershad, F. et al. Ultra-conformal drawn-on-skin electronics for multifunctional motion artifact-free sensing and point-of-care treatment. *Nat. Commun.* **11**, 3823 (2020).
19. Ferrari, L. M. et al. Ultraconformable temporary tattoo electrodes for electrophysiology. *Adv. Sci.* **5**, 1700771 (2018).
20. Xu, Y. et al. Pencil–paper on-skin electronics. *Proc. Natl Acad. Sci. USA* **117**, 18292–18301 (2020).
21. Tian, L. et al. Flexible and stretchable 3ω sensors for thermal characterization of human skin. *Adv. Funct. Mater.* **27**, 1701282 (2017).
22. Crawford, K. E. et al. Advanced approaches for quantitative characterization of thermal transport properties in soft materials using thin, conformable resistive sensors. *Extrem. Mech. Lett.* **22**, 27–35 (2018).
23. He, H. et al. Biocompatible conductive polymers with high conductivity and high stretchability. *ACS Appl. Mater. Int.* **11**, 26185–26193 (2019).
24. Oh, J. Y. et al. Effect of PEDOT nanofibril networks on the conductivity, flexibility, and coatability of PEDOT:PSS films. *ACS Appl. Mater. Int.* **6**, 6954–6961 (2014).
25. Kim, E., Xia, Y. & Whitesides, G. M. Micromolding in capillaries: applications in materials science. *J. Am. Chem. Soc.* **118**, 5722–5731 (1996).
26. Blümel, A. et al. Micromolding in capillaries and microtransfer printing of silver nanoparticles as soft-lithographic approach for the fabrication of source/drain electrodes in organic field-effect transistors. *Org. Electron.* **8**, 389–395 (2007).
27. White, S. I. et al. Electrical percolation behavior in silver nanowire–polystyrene composites: simulation and experiment. *Adv. Funct. Mater.* **20**, 2709–2716 (2010).
28. Mutiso, R. M., Sherrott, M. C., Rathmell, A. R., Wiley, B. J. & Winey, K. I. Integrating simulations and experiments to predict sheet resistance and optical transmittance in nanowire films for transparent conductors. *ACS Nano* **7**, 7654–7663 (2013).
29. Sun, Y., Yin, Y., Mayers, B. T., Herricks, T. & Xia, Y. Uniform silver nanowires synthesis by reducing AgNO3 with ethylene glycol in the presence of seeds and poly(vinyl pyrrolidone). *Chem. Mater.* **14**, 4736–4745 (2002).
30. Andres, L. J. et al. Rapid synthesis of ultra-long silver nanowires for tailor-made transparent conductive electrodes: proof of concept in organic solar cells. *Nanotechnology* **26**, 265201 (2015).
31. Yao, S. & Zhu, Y. Wearable multifunctional sensors using printed stretchable conductors made of silver nanowires. *Nanoscale* **6**, 2345–2352 (2014).
32. Xu, Y. et al. Multiscale porous elastomer substrates for multifunctional on-skin electronics with passive-cooling capabilities. *Proc. Natl Acad. Sci. USA* **117**, 205–213 (2020).
33. Liu, L. et al. Silicone-based adhesives for long-term skin application: cleaning protocols and their effect on peel strength. *Biomed. Phys. Eng. Express* **4**, 015004 (2017).
34. Jang, K.-I. et al. Rugged and breathable forms of stretchable electronics with adherent composite substrates for transcutaneous monitoring. *Nat. Commun.* **5**, 4779 (2014).
35. Wang, Y. et al. Epidermal electrodes with enhanced breathability and high sensing performance. *Mater. Today Phys.* **12**, 100191 (2020).
36. Oyen, M. L. Mechanical characterisation of hydrogel materials. *Int. Mater. Rev.* **59**, 44–59 (2014).

37. Ní Annaidh, A., Bruyère, K., Destrade, M., Gilchrist, M. D. & Otténio, M. Characterization of the anisotropic mechanical properties of excised human skin. *J. Mech. Behav. Biomed. Mater.* **5**, 139–148 (2012).
38. Jeong, J.-W. et al. Materials and optimized designs for human–machine interfaces via epidermal electronics. *Adv. Mater.* **25**, 6839–6846 (2013).
39. Thakor, N. V. & Zhu, Y. Applications of adaptive filtering to ECG analysis: noise cancellation and arrhythmia detection. *IEEE Trans. Biomed. Eng.* **38**, 785–794 (1991).
40. Jeong, J.-W. et al. Materials and optimized designs for human–machine interfaces via epidermal. *Electronics* **25**, 6839–6846 (2013).
41. Huynh, T. H., Jafari, R. & Chung, W. Y. An accurate bioimpedance measurement system for blood pressure monitoring. *Sensors-Basel* **18**, 2095 (2018).
42. Ibrahim, B., McMurray, J. & Jafari, R. A wrist-worn strap with an array of electrodes for robust physiological sensing. *Annu. Int. Conf. IEEE Eng. Med. Biol. Soc.* **2018**, 4313–4317 (2018).
43. Sodolski, T. & Kutarski, A. Impedance cardiography: a valuable method of evaluating haemodynamic parameters. *Cardiol. J.* **14**, 115–126 (2007).
44. Nichols, W. W. Clinical measurement of arterial stiffness obtained from noninvasive pressure waveforms. *Am. J. Hypertens.* **18**, 3S–10S (2005).

ACKNOWLEDGEMENTS

The authors acknowledge the funding from the Department of Biomedical Engineering at Texas A&M University, the Texas A&M Engineering Experiment Station, the National Science Foundation (Grant No. 1648451), and the National Institutes of Health (Grant No. 1R21EB029064-01A1). In addition, the use of the Texas A&M Materials Characterization and Soft Matter Facility is acknowledged.

AUTHOR CONTRIBUTIONS

L.T. conceived the idea. M.N. and L.T. designed the project, experiments and wrote the manuscript. H.G. and Md.S.R. helped with materials characterization. D.W., C.P., and S.H. helped with sample preparation and human subject measurements. All authors reviewed the manuscript.

COMPETING INTERESTS

L.T. and M.N. are inventors on an International Patent Application (No. PCT/US22/18015) related to this work filed by the Texas A&M University System. The other authors declare that they have no competing interests.

ADDITIONAL INFORMATION

Supplementary information The online version contains supplementary material available at https://doi.org/10.1038/s41528-022-00170-y.

Correspondence and requests for materials should be addressed to Limei Tian.

Reprints and permission information is available at http://www.nature.com/reprints

Publisher's note Springer Nature remains neutral with regard to jurisdictional claims in published maps and institutional affiliations.